

RESEARCH ARTICLE

10.1002/2017WR020450

Direct Breakthrough Curve Prediction From Statistics of Heterogeneous Conductivity Fields

Scott K. Hansen¹ , Claus P. Haslauer² , Olaf A. Cirpka² , and Velimir V. Vesselinov¹ 

¹Computational Earth Sciences Group (EES-16), Los Alamos National Laboratory, Los Alamos, NM, USA, ²Center for Applied Geoscience, University of Tübingen, Tübingen, Baden-Württemberg, Germany

Key Points:

- Lognormal breakthrough curve parameters fitted as functions of variance of log-hydraulic conductivity and distance to source
- Estimates are calculated for error of predicted flux-weighted breakthrough curves and coherence of point breakthrough curves
- Macrodispersion coefficients are derived for highly heterogeneous media using a breakthrough time-based approach

Supporting Information:

- Supporting Information S1
- Data Set S1

Correspondence to:

S. K. Hansen,
skh3@lanl.gov

Citation:

Hansen, S. K., Haslauer, C. P., Cirpka, O. A., & Vesselinov, V. V. (2018). Direct breakthrough curve prediction from statistics of heterogeneous conductivity fields. *Water Resources Research*, 54, 271–285. <https://doi.org/10.1002/2017WR020450>

Received 19 JAN 2017

Accepted 22 DEC 2017

Accepted article online 4 JAN 2018

Published online 23 JAN 2018

Abstract This paper presents a methodology to predict the shape of solute breakthrough curves in heterogeneous aquifers at early times and/or under high degrees of heterogeneity, both cases in which the classical macrodispersion theory may not be applicable. The methodology relies on the observation that breakthrough curves in heterogeneous media are generally well described by lognormal distributions, and mean breakthrough times can be predicted analytically. The log-variance of solute arrival is thus sufficient to completely specify the breakthrough curves, and this is calibrated as a function of aquifer heterogeneity and dimensionless distance from a source plane by means of Monte Carlo analysis and statistical regression. Using the ensemble of simulated groundwater flow and solute transport realizations employed to calibrate the predictive regression, reliability estimates for the prediction are also developed. Additional theoretical contributions include heuristics for the time until an effective macrodispersion coefficient becomes applicable, and also an expression for its magnitude that applies in highly heterogeneous systems. It is seen that the results here represent a way to derive continuous time random walk transition distributions from physical considerations rather than from empirical field calibration.

1. Introduction

It is widely recognized that solute transport in real aquifers is characterized by asymmetric plumes and heavy-tailed breakthrough curves. This behavior may be advection driven (created by neighboring stream tubes with significantly different velocities; e.g., Ederly et al., 2014), or diffusion driven (caused by mobile-immobile trapping processes that sever the link between advection and transport; e.g., Haggerty et al., 2000). In this paper, we consider the former mechanism.

Macrodispersion theory represented the first attempt to model such conditions. This theory is based on implicitly smoothing heterogeneous media to an equivalent homogeneous continuum, and then adding an artificial Fickian dispersion term to capture the scattering effects of the disregarded heterogeneity. The practical motivation for this maneuver is the impossibility of characterizing small-scale heterogeneity. The central limit theorem provides justification for attempting such a characterization in some cases, as large particle motions may be considered as the sum of smaller motions, and if these motions are considered as independent draws from the same distribution, their sum will have a Gaussian distribution. This sum distribution (representative of relative plume concentration) may thus be described by an equivalent Fickian model. Classic papers of the early 1980s (Dagan, 1982; Gelhar & Axness, 1983) derived the corresponding coefficients by small-perturbation analysis, following on earlier numerical research (e.g., Schwartz, 1977).

In stationary, heterogeneous, 3-D hydraulic conductivity (K) fields, Gelhar and Axness (1983) employed spectral techniques to determine a macrodispersion coefficient in terms of the Eulerian velocity covariance structure and to express this in terms of the spatial covariance structure of the log-hydraulic conductivity field. We denote this covariance function by $C_{\ln K}(\Delta x)$, where K stands for hydraulic conductivity and Δx for the separation distance. For different domains in which the Fourier transform of the Eulerian velocity covariance structure may be calculated analytically, different macrodispersion coefficients may be computed. A limitation of this theory is its assumption of small perturbations in the concentration (Rubin, 2003, p. 178), regardless of the assumptions underlying the computation of the Eulerian velocity covariance. An alternative approach, based on Lagrangian ideas, does not explicitly make small-concentration-fluctuation assumptions. Many explicit solutions have been derived using this framework (e.g., Dagan, 1989). However,

the Lagrangian velocity covariance structure is difficult to measure directly or to compute (Woodbury & Rubin, 2000), and it is often rewritten as function of the macroscopic mean groundwater velocity and the Eulerian velocity covariance structure. This itself embeds a small variance assumption (Rubin, 2003, p. 219).

It should thus be clear that, despite the variety of different analytical solutions in the literature, there are two major problems implicit in the use of the macrodispersion ideas, even assuming that $C_{\ln K}(\Delta_x)$ is known and aquifer statistics are stationary. First, moderately heterogeneous aquifers for which $\sigma_{\ln K}^2 \equiv C_{\ln K}(0) > 1$ are common in practical hydrogeology, invalidating small-fluctuation assumptions. Second, Fickian behavior will only be observed after some time, and behavior before this point will appear anomalous (Dentz et al., 2004). Some work has been done on both of these questions.

Interest in arbitrarily large values of $\sigma_{\ln K}^2$ has existed for a long time. One approach has been simply to ignore $\sigma_{\ln K}^2$, and to use regression analysis to seek an empirical relationship between distance from source and effective macrodispersivity (see e.g., Zech et al., 2015, and works cited therein). However, this approach has not led to a strong general relationship (although different, more consistent relationships were found by Zech et al. (2015) at individual sites). Other authors have used a combination of analytical and numerical approaches to specifically study macrodispersion coefficients for larger $\sigma_{\ln K}^2$. Neuman and Zhang (1990) employed mathematical arguments pointing to a linear increase in the late-time-effective macrodispersion coefficient as a function of $\sigma_{\ln K}^2$, although subsequent studies have gone against this. Bellin et al. (1992) indicated an Eulerian velocity covariance that increased faster than linearly with $\sigma_{\ln K}^2$. Salandin and Fiorotto (1998) were among the first to employ numerical simulations, observing the implied macrodispersion coefficients for values of $\sigma_{\ln K}^2$ up to 4. Their simulations covered only early time, and they did not find late-time asymptotic values of the macrodispersivity: they considered times up to dimensionless time $T = 20$, where T is defined as $T \equiv \frac{tU}{l_{\ln K}}$. Here t is travel time since solute release, U is average groundwater velocity in the principal direction, and $l_{\ln K}$ is the integral scale of the spatially distributed K -field. T may be thought of as the number of integral scales traveled by the plume centroid in time t . Another approach to this problem has been the so-called *self-consistent approach* (e.g., Cvetkovic et al., 2014; Dagan et al., 2003; Di Dato et al., 2016), which assumes that the aquifer is an effectively homogeneous medium with spheroidal or cuboidal inclusions of different hydraulic conductivity. Subject to a number of approximations, this approach makes it possible to formally write the longitudinal macrodispersivity as a multidimensional integral over the joint pdf of inclusion radius and conductivity and the asymptotic trajectory deflection due to a single such inclusion (Dagan et al., 2003).

Authors have differed greatly on the length of time necessary to reach “late time,” and for macrodispersivities to converge. A pair of early analytical and numerical studies (Dentz et al., 2000, 2002) found, for $\sigma_{\ln K}^2 = 1$, that the macrodispersivity stabilized at $T = 50$. Janković et al. (2003) performed a numerical particle tracking study in a 3-D model with spherical inclusions, found that macrodispersivity had stabilized by $T = 40$, for $\sigma_{\ln K}^2 \leq 4$. Trefry et al. (2003) did partial differential equation (PDE) simulations in 2-D for several individual realizations with high local-scale dispersivity (local-scale Peclet number, $Pe \equiv \frac{l_{\ln K}}{\alpha}$, of 10–20), finding that even at $T > 300$, the asymptotic state may not have been reached, although for variances $2.5 \leq \sigma_{\ln K}^2 \leq 4$ this state was apparently obtained by that point. (In this document, we use the term *local-scale dispersion* to refer to dispersive processes below the scale at which the velocity field is discretized.) Trefry et al. (2003) also compared the entropy of the plumes in 2-D and found that plumes remained far from Gaussian (although this is a stricter criterion than Gaussian entropy viewed only in 1-D or linear increase of second-central spatial moments with time). Beaudoin and De Dreuzy (2013) performed many 3-D particle tracking simulations and tabulated ensemble particle spatial variances over time from the numerical results. From the rates of change, longitudinal macrodispersivities were estimated. These were found to stabilize between $T = 10$ for $\sigma_{\ln K}^2 = 1$ and $T = 100$ for $\sigma_{\ln K}^2 = 4$.

Macrodispersion, like local-scale dispersion, is an amplification process in which the effect of smaller-scale scattering is increased by the proximity of nearby streamlines with different velocities (Werth et al., 2006). In the limit of no local-scale dispersion, the distribution of breakthrough times at a plane is purely determined by the flux-weighted transit time distribution for the individual stream tubes. In the other limit, extremely large values of “local-scale” dispersion dominate any macrodispersive effects, and the macrodispersion equals the local-scale dispersion. Literature studies have considered finite Pe that range from approximately 10 (Trefry et al., 2003) to 10,000 (Srzić et al., 2013), and some (e.g., Beaudoin & De Dreuzy, 2013; Janković et al., 2003) have considered no local-scale dispersion, implying $Pe = \infty$. Srzić et al. (2013) reported that that

Pe was important for the time until the plume becomes ergodic (Dagan & Fiori, 1997; Fiori, 1996). However, for longitudinal macrodispersion, Dentz et al. (2002) considered local-scale dispersion ranging 4 orders of magnitude above that of pure diffusion and $\sigma_{\ln K}^2 = 1$ and found only small sensitivity of the macrodispersion coefficient to the local-scale dispersion strength. Similarly, Janković et al. (2003) found, for $\sigma_{\ln K}^2 \leq 4$, little effect of local-scale dispersion.

So far, we have mentioned studies analyzing the spatial spread of solute clouds that are released at time zero. Another perspective of potential interest in practical applications is breakthrough curve analysis, considering the passage of particles at a fixed plane downgradient of the source. Early semianalytic work in this direction, for aquifers with small variability, was performed by Cvetkovic et al. (1992) and Dagan et al. (1992). Bellin et al. (1994) continued this analysis numerically. Trefry et al. (2003) also considered breakthrough curves at control planes in 2-D domains and found that these were well described by a Fickian model, even at centroid travel distances for which the 2-D plume was significantly non-Gaussian. Gotovac et al. (2009) performed a numerical particle tracking study which considered breakthrough curves at multiple planes and showed breakthrough curves were well described by lognormal distributions for values of $\sigma_{\ln K}^2 < 4$, with performance degrading gradually in the late-time tail for larger degrees of heterogeneity. Lognormal breakthrough distributions have also recently been endorsed for non-Gaussian (persistent and antipersistent) correlation structures (Moslehi & de Barros, 2017).

Given the potentially long travel times and distances until a macrodispersive model is valid, as well as the fact that the aquifer needs to be statistically stationary over a substantially larger scale, recent efforts have focused on upscaling techniques that capture the behavior of the preasymptotic regime. Modeling transport with the continuous time random walk (CTRW) method (Berkowitz et al., 2006) is a technique that has proven successful for preasymptotic behavior (e.g., Dentz et al., 2004; Levy & Berkowitz, 2003; Rubin et al., 2012). CTRW is also applicable to 1-D approximations of advective solute transport, with early consideration being seen in Margolin and Berkowitz (2004). Such a 1-D CTRW was explicitly proposed as an upscaling framework—the so-called RP-CTRW—for flow in heterogeneous aquifers by Hansen and Berkowitz (2014). In this approach, solute transport is fully described by a parameterized travel-time distribution from one observation plane to the next, and breakthrough curves at distances of several observation planes are obtained by convolving the travel-time distribution with itself. The latter authors also showed the predictive nature of the CTRW in that context, demonstrating consistency in the CTRW transition distributions that best matched breakthrough curves at several planes at different distances from a source in a single model. This conclusion was reinforced by Fiori et al. (2015), through reanalysis of another data set. They again found that CTRW parameters calibrated from early breakthrough locations well matched breakthrough at downgradient locations.

In the following, we will, informed by knowledge of the predictive nature of plane-to-plane CTRW transition, per Hansen and Berkowitz (2014), and lognormality of breakthrough, per Gotovac et al. (2009), seek to ground this lognormal distribution in conductivity statistics. In this way, we seek to combine the predictive nature of the macrodispersion theory (which may be used to predict breakthrough based on conductivity field statistics but has been limited to mildly heterogeneous aquifers and/or late time) and the more recent CTRW theory (which has demonstrated excellent performance at capturing realistic behavior in a range of circumstances, but which has not been fit predictively).

We approach this task from a computational perspective, running particle tracking simulations on multiple realizations, collecting statistics, and performing a modified polynomial regression to determine the best descriptive model. In particular, the log-variance of the breakthrough curve shape is expressed as a function of two parameters of a locally isotropic, lognormally distributed hydraulic conductivity field with an exponential semivariogram. While isotropy is not characteristic of natural media, it has been found that the longitudinal particle displacement variance underlying longitudinal macrodispersion is insensitive to the transverse anisotropy (Rubin & Ezzedine, 1997), and isotropy is thus a common assumption to make in numerical studies of macrodispersive processes (e.g., Beaudoin & De Dreuzy, 2013; Cvetkovic et al., 1996; Dentz et al., 2002). The multi-Gaussian assumption has been used in virtually all the aforementioned numerical studies, but its effect has not been quantified; this analysis is saved for a follow-up study. The two predictive parameters considered are the integral scale and the log-variance of the conductivity field. Using data from the multiple realizations, we also consider the intrarealization variability of the breakthrough curves for point sources at different locations, and the consequent degree of predictive power that the regression possesses for these.

Other goals of this paper include computationally evaluating late-time macrodispersion coefficients based on our simulations, determining heuristics for onset of “late time” in this context, and evaluating previously proposed models for macrodispersion coefficients. In the CTRW context, our regression allows prediction of transition distributions in the upscaled, discretized RP-CTRW framework, which may be of use in the upscaling of field-scale transport. Our analysis also provides support for the idea that truncated (or tempered) power laws are fundamental, and arise as a natural generalization of the macrodispersion theory.

In section 2, we develop the theoretical ideas underpinning our analysis and show how it relates mathematically to both the macrodispersion and the CTRW theories. In section 3, we describe our numerical procedure. In section 4, we discuss the results of our statistical analyses. Finally, in section 5, we summarize our findings and make suggestions for future work.

2. Theory

In this section, we discuss results from two bodies of theory—the macrodispersion theory and the CTRW theory—and discuss how our contributions relate to both.

2.1. Relationship to the Macrodispersion Theory

In effectively homogeneous media, it has long been established (Kreft & Zuber, 1978, equation 11) that, for instantaneous release in flux and detection in flux, the flux concentration, c_f , satisfies the equation

$$\frac{nU}{M} c_f(x, t) = \frac{x}{t} \left[\frac{1}{(4\pi Dt)^{\frac{1}{2}}} \exp \left\{ -\frac{(x-Ut)^2}{4Dt} \right\} \right], \tag{1}$$

where x is the distance downgradient from the release location, t is time since release, D is an effective dispersion coefficient, U is the mean groundwater velocity, n is the porosity, and M is the amount of solute injected per unit area transverse to mean flow. The right-hand side of (1) can be considered as proportional to a pdf (corresponding to an inverse Gaussian distribution) of t . This pdf has known expected value μ_t and variance σ_t^2 (Kreft & Zuber, 1978):

$$\mu_t \equiv \frac{x}{U}, \tag{2}$$

$$\sigma_t^2 = \frac{2Dx}{U^3}. \tag{3}$$

Consider the statistics of breakthrough at a given plane x units downgradient of another parallel plane from which particles are randomly released in a flux-weighted fashion at time 0, and imagine that we desire to determine the macrodispersion coefficient, D_∞ , using relationships given above. For coherence with existing notation, we will let $D_\infty = D$. Then, combining (2) and (3) yields

$$D_\infty = \frac{\sigma_t^2 x^2}{2\mu_t^3}. \tag{4}$$

From this, it follows that if an empirical breakthrough curve is well modeled by an inverse Gaussian distribution, it is possible to infer the implied macrodispersion coefficient.

As mentioned, other authors have argued that the lognormal distribution well describes particle breakthrough over a wide range of subsurface heterogeneities, up to about $\sigma_{\ln K}^2 = 4$. For small log-variances ($\sigma_{\ln t}^2 \leq 0.5$), and we refer here to the log-variances of travel time, *not* K , the lognormal and inverse Gaussian distributions are essentially identical. By this is meant: if a large number of draws are taken from a lognormal distribution with moderate log-variance, the inverse Gaussian pdf matching the empirical mean and variance will be near-identical to the lognormal pdf from which the samples were drawn. On account of the central limit theorem, one would expect the log-variance of breakthrough curves to decrease (i.e., symmetry to increase) with increasing distance from the source, and thus for the calibrated lognormal breakthrough curve to imply an effective D_∞ , via (4).

For small $\sigma_{\ln K}^2$, at late time in a 3-D isotropic medium with an exponential covariance structure, it is a classic result (see e.g., Rubin, 2003, equation 10.19) that the following relationship holds

$$D_{\infty} = \sigma_{\ln K}^2 l_{\ln K} U. \quad (5)$$

It is interesting to verify the degree to which this small-heterogeneity approximate macrodispersion coefficient relates to the empirical one from the regression, as a function of $\sigma_{\ln K}^2$. We consider this matter in section 4.4, and at length in Appendix B.

2.2. Relationship to CTRW Theory

The CTRW paradigm (Berkowitz et al., 2006) is known as a means of capturing realistic solute transport, including transport with heavy-tailed breakthrough curves or asymmetrical plumes. Hansen and Berkowitz (2014) argued that for advection-dominated anomalous transport in heterogeneous media, essentially all information about breakthrough curves is encoded in a point-to-point transition time pdf, $\psi(t)$. This approach has also previously been proposed (as the *time domain random walk*) as a numerical method for solving Fickian transport problems (Banton et al., 1997) and for transition of fracture network sections (Delay & Bodin, 2001). Within this approach, we consider a fixed transition distance, $\Delta \mathbf{x}$, greater than the correlation length of the velocity field (which, per Fiori & Jankovic, 2012, may be significantly larger than the correlation length of the K -field), and model the solute behavior by a random walker whose position in space and time after the n th transition, (\mathbf{x}_n, t_n) , is updated via the following relations:

$$\mathbf{x}_{n+1} = \mathbf{x}_n + \Delta \mathbf{x}, \quad (6)$$

$$t_{n+1} = t_n + \Delta t_n, \quad (7)$$

where each Δt_n is a random time increment drawn from the same pdf, ψ :

$$\Delta t_n \sim \psi(t; \Delta \mathbf{x}). \quad (8)$$

Provided that $\psi(t)$ is sufficient to determine breakthrough curves at arbitrary locations, the question of which functional form corresponds to realistic behavior arises. Recent papers have argued the fundamental form of ψ is a power law with exponential tempering. In a systematic particle tracking study under a variety of statistical conditions, Edery et al. (2014) showed that this form well described the histogram of flux-weighted transition times across small intervals (they fit what is known as a *truncated power law*; a shifted Pareto distribution with exponential tempering). Similarly, in a survey of hydrologic models for point-to-point breakthroughs, Cvetkovic (2011) argued that essentially all probability models in current use were of the same form, with power law tails and late-time exponential tempering, although Cvetkovic et al. (2014) present a specific system architecture for which they argue such models are not appropriate.

We concur with the recent assessment that power laws with exponential tailing are fundamental and show how they are actually apparent in what is seemingly a completely “classical” problem: solution of the advection dispersion equation with an instantaneous solute release for breakthrough at a location downgradient. In fact, as we show in Appendix A for small Peclet numbers (1) has a truncated power law tail. Thus, it is reasonable to attempt to understand (moderately) heterogeneous advective transport phenomena by both CTRW and classical techniques.

In the macrodispersion context of section 2.1, the breakthrough curve shape was tied to D_{∞} , which is in turn tied (under mild K -field variability) to subsurface parameters. We desire to accomplish the same sort of prediction for $\psi(t)$ in terms of subsurface parameters, under more general conditions: either prior to the applicability of the macrodispersion regime, or in it, but for large $\sigma_{\ln K}^2$ which are not covered by (5). Note that for a fixed location, $U c_f$ and ψ both represent temporal arrival time distributions. Thus, provided $\Delta \mathbf{x}$ is much greater than the velocity correlation length (implying $\Delta \mathbf{x} \gg l_{\ln K}$), there is a simple relationship between the two:

$$\psi(t; \Delta \mathbf{x}) = \frac{nU}{M} c_f(\Delta \mathbf{x}, t). \quad (9)$$

3. Numerical Analysis

The numerical experiments at the heart of this study are performed in simulated 3-D domains containing a heterogeneous, locally isotropic hydraulic conductivity field. Eighty conductivity field realizations are created for the study, all using the same basic computational technique. Each conductivity field realization is a box with length $L_x = 200$ m in the x_{box} direction, length $L_y = 50$ m in the y_{box} direction, and length

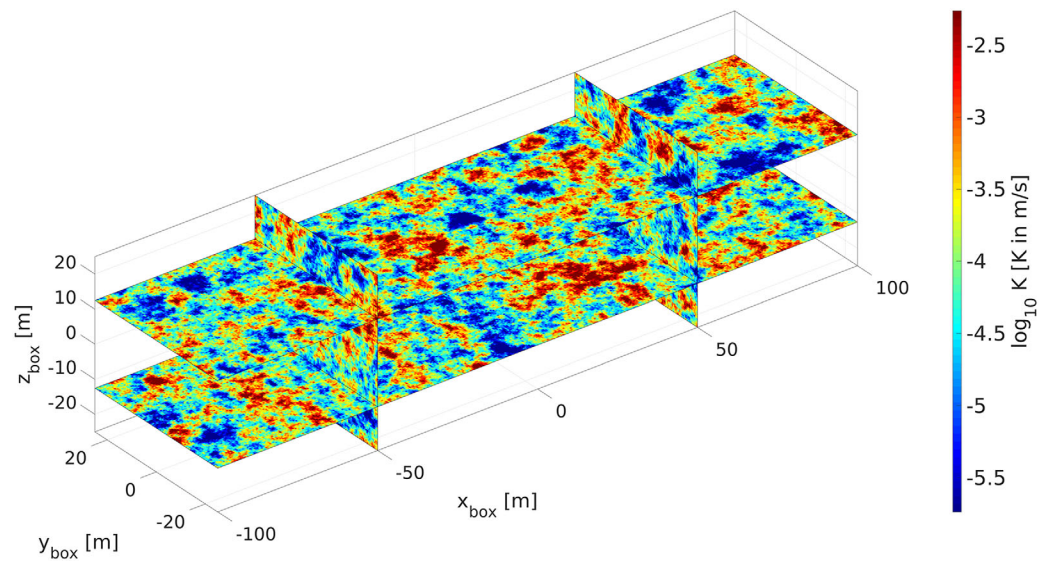


Figure 1. Example realization of a single box in the case of $\sigma_{\ln K}^2=4$.

$L_z = 50$ m in the z_{box} direction, is divided into 0.5 m cubic cells, each of which is assigned a spatially distributed $\ln K$ value based on multivariate normally simulated, spatially periodic realizations (Dykaar & Kitanidis, 1992). Figure 1 shows an example realization.

The hydraulic conductivity in each cubic cell of the box representing a single conductivity field is drawn from a lognormal distribution. The geometric mean of K is $1\text{E-}4$ m/s, and the log-variance is fixed for any given realization. The target spatial covariance structure is described by an exponential semivariogram with target an integral scale, $l_{\ln K}$, of 3.33 m in all directions, whose actual value varies slightly between realizations. The semivariogram, γ , is mathematically defined according to

$$\gamma(h) = \sigma_{\ln K}^2 \left[1 - \exp\left(-\frac{h}{l_{\ln K}}\right) \right], \quad (10)$$

where h is the separation distance between two points. Note that periodicity implies that $\gamma(L_i+h) = \gamma(h)$, where i stands in for x , y , or z . We ensure periodicity in all three spatial directions. We apply periodic boundary conditions with a trend in the mean. That is, for any two opposite faces of the box, each pair of opposing points on those faces has the same head drop between them as every other pair of opposing points on those same faces. For clarity: opposing points on the two faces defined by $x_{\text{box}} = -100$ and $x_{\text{box}} = 100$ are those with the same coordinates $(y_{\text{box}}, z_{\text{box}})$ on each of those faces, and similarly for other opposing pairs of faces. The head drop between each opposing pair of faces is adjusted so that the mean advection velocity, U , is purely in the x direction, and has magnitude $1\text{E-}6$ m/s. A porosity of 0.3 is assumed.

One may imagine filling space by endlessly repeating this box, “gluing” together opposite faces in such a way that all opposing points are identified, to create a 3-D-periodic structure whose period in each direction is equal to the length of the box in that direction, aligning the local $(x_{\text{box}}, y_{\text{box}}, z_{\text{box}})$ coordinate system in each box with the global (x, y, z) coordinate system. The flow field derived from solving the groundwater flow equation on the box under periodic boundary conditions is valid throughout space, and one does not have to be concerned with the effects of no-flow or fixed-head boundary conditions, as in other approaches.

In such a periodic environment, particle tracking may be performed using only the single box described initially: when a particle travels outward through a point on a boundary of the box in the i direction, it is moved to the opposing point on the opposite face and continues its motion, with its global coordinate incremented or decremented by L_i , as appropriate. The particle is imagined as “really” being in the unbounded global coordinate system, but for simulation purposes never leaves the box.

Particle tracking is performed using the semianalytical method of Pollock (1988). Each single transition consists of pure advection along a streamline until the particle reaches a cubic cell boundary, followed by a dispersive motion in the y and z directions. The magnitude of each of these transverse dispersive motions is determined by a draw from the distribution $N(0, 2\alpha\Delta_x)$, where Δ_x is the distance traveled by pure advection in the x direction during the current transition, and α , the pore-scale transverse dispersivity, is always 5E-4 m. For clarity, we may explicitly write the particle position update equation as

$$\mathbf{x}_{n+1} = \mathbf{x}_n + \Delta\mathbf{x}_n + \zeta_1\mathbf{j} + \zeta_2\mathbf{k}, \quad (11)$$

where \mathbf{x}_n represents the particle position after the n th transition, $\Delta\mathbf{x}_n$ represents the advective motion on the n th transition, \mathbf{j} and \mathbf{k} are the respective y and z coordinate unit vectors, and $\zeta_1 \sim \zeta_2 \sim N(0, 2\alpha\Delta_x)$. The addition of local-scale dispersion makes breakthrough times for particles released at the same location nondeterministic and allows for analysis of breakthrough statistics as a function of release location.

For each realization of the K -field, particle tracking is performed by releasing 40 particles from each of the center points of the 10,000 upgradient faces of the cubic cells that lie on each of 10 planes orthogonal to the mean flow velocity (with locations $x_{\text{box}} = 20n - 120$, for $n = 1$ to 10). For each particle, the plane on which it is released is identified with $x = 0$ in the global coordinate system. Each particle is tracked downgradient until its "global" x coordinate reaches L_x . Each particle's first passage of the 25 planes located at $x = \frac{nL_x}{25}$ units downgradient of its release location, $n = 1-25$, its arrival time is recorded, along with its release location (plane index, y_{box} , and z_{box}). The purpose behind performing multiple flux-weighted releases at planes, each separated by multiple integral scales, within a single K -field realization is to increase the number of "effective realizations" for calibration of early-time behavior.

A set of eight variances, $\sigma_{\ln K}^2 \in [0.5, 4]$, linearly spaced in the interval and including both end points, are used to simulate ten realizations of K , for a total of 80 distinct particle tracking simulations performed.

All simulations are performed using a MATLAB code which we have made available in the supporting information of the article. To accelerate the particle tracking, we perform the relevant calculations on GPUs, using the capabilities of the MATLAB Parallel Computing Toolbox.

The breakthrough data from these simulations were used for the statistical analyses that underpin the claims of the paper. Three separate analyses are performed:

1. Point breakthrough curve coherence (this is to say, the dependence of breakthrough curve statistics on release location) is analyzed.
2. A regression is performed against variance of the $\ln K$ field and the dimensionless distance from the source, $X \equiv x/l_{\ln K}$, with the aim of *predicting* flux-averaged breakthrough curves. This regression is based on the following observations regarding breakthrough curves:
 - a. They are well described by lognormal distributions (Gotovac et al., 2009). We also verified this using our data set (see Appendix C).
 - b. The (dimensional) mean arrival time at distance x downgradient is well described by $\mu_t (= \frac{x}{U})$, for $X \gg \sigma_{\ln K}^2$, where U is computed by Darcy's law using the geometric mean hydraulic conductivity (Guadagnini, 2003). Verification of this result using our data set is shown in Appendix B.
 - c. All else being equal, with greater heterogeneity of the $\ln K$ field, breakthrough curves are *less* symmetrical (variance of the log breakthrough time is larger). All else being equal, with greater distance from the release location, breakthrough curves are *more* symmetrical (variance of the log breakthrough time is smaller).
3. The required travel distance until an ADE analysis with an effective macrodispersion coefficient can be used is assessed, using the theory developed in section 2.1 and Appendix B.

4. Results and Discussion

4.1. Predictive Regression

As K -field variability and distance from source are expected to be determinants of breakthrough behavior, it is reasonable to attempt to predict $\sigma_{\ln t}^2$, the variance of the natural logarithm of (flux-weighted) particle arrival times which defines the lognormal breakthrough curve, as a function of $\sigma_{\ln K}^2$ and X . We approach this

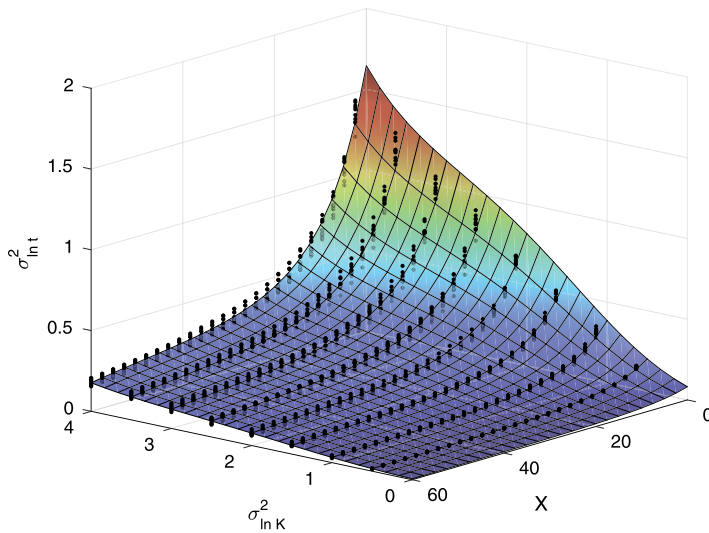


Figure 2. Regression for In-variance of breakthrough curve as a function of X and $\sigma_{\ln K}^2$: 3-D view of regression surface shown along with the data points used to train it.

problem by means of polynomial regression. We compute the variances of the natural logarithm of (flux-weighted) particle arrival times at each of the planes at which breakthrough was recorded, for each of the ten K -field realizations, for each of the eight K -field heterogeneity levels. These are plotted as 3-D scatter points in Figure 2. A third-order bivariate polynomial regression of natural logarithm of these variances is computed against X and $\sigma_{\ln K}^2$. We thus arrive at the predictive relationship

$$\sigma_{\ln t}^2(X; \sigma_{\ln K}^2) = \exp \left\{ \sum_{i=0}^3 \sum_{j=0}^3 c_{ij} \sigma_{\ln K}^{2i} X^j \right\}, \quad (12)$$

where i and j represent the powers of $\sigma_{\ln K}^2$ and X employed in the polynomial regression, and whose fitted coefficients, c_{ij} , are compiled in Table 1. The order of the regression is arbitrary, and is selected because it is the lowest power that qualitatively appears to give a good fit to the data. The regression surface (i.e., the surface defined by (12)) is also shown in Figure 2.

The mean breakthrough time for a particle, independent of $\sigma_{\ln K}^2$, is well described by x/U (Guadagnini, 2003). Combining this with our presumption of lognormality of breakthrough curves, we predict

that the breakthrough curve at distance x from the source for a Dirac upgradient boundary condition, $\frac{nU}{M} c_f(0, t) = \delta(t)$, satisfies

$$\frac{nU}{M} c_f(x, t) = \frac{1}{t \left(2\pi \sigma_{\ln t}^2 \left(\frac{x}{\ln K} \right) \right)^{\frac{1}{2}}} \exp \left\{ - \frac{\left(\ln t - \ln \frac{x}{U} + \frac{1}{2} \sigma_{\ln t}^2 \left(\frac{x}{\ln K} \right) \right)^2}{2 \sigma_{\ln t}^2 \left(\frac{x}{\ln K} \right)} \right\}. \quad (13)$$

This is to say, the breakthrough curve is the pdf for $\ln N \left(\ln \frac{x}{U} - \frac{1}{2} \sigma_{\ln t}^2 \left(\frac{x}{\ln K} \right), \sigma_{\ln t}^2 \left(\frac{x}{\ln K} \right) \right)$. Equation (13) can also be rewritten in terms of the dimensionless variables X and T :

$$\frac{nU}{M} c_f(X, T) = \left[\frac{U}{\ln K} \right] \frac{1}{T \left(2\pi \sigma_{\ln t}^2(X) \right)^{\frac{1}{2}}} \exp \left\{ - \frac{\left(\ln X - \ln T + \frac{1}{2} \sigma_{\ln t}^2(X) \right)^2}{2 \sigma_{\ln t}^2(X)} \right\}, \quad (14)$$

where only the square-bracketed component is dimensional (required because $\frac{nUc_f}{M}$ is a temporal density). Note that the right-hand side is proportional to the plane-to-plane transition time pdf, defining an RP-CTRW (or TDRW) transition time distribution for transitions of fixed length, X . The various $\sigma_{\ln t}^2$ are plotted as 3-D scatter points, superimposed on the calibrated regression surface in Figure 2.

4.2. Independence of Release Location

It is unlikely that a solute source is uniformly distributed over a plane, and much more likely that there is a quasi-point source (spatially localized in all dimensions, and of a maximum scale that is small with respect to the distance from the breakthrough location of interest to the centroid of the source). For predictive modeling, we would like to establish the degree to which a breakthrough curve at a given compliance plane is affected by the release location.

It is intuitive that, with increasing distance from the source, a particle will sample more of the heterogeneity, and the release location will have less impact on the shape of the breakthrough curve. At the same time, one might expect that in more heterogeneous media, for any given distance from the source, there will be more dependence on release locations (as there is more variability to sample before ergodicity is achieved). Our investigations bear out those qualitative predictions. Figure 3 shows individual point-release breakthrough curves for different degrees of K -field heterogeneity and distances from the source, expressed as cumulative distribution functions (CDF). To provide more quantitative guidance, we compute coherence statistics

Table 1
Third-Degree Polynomial Regression Coefficients c_{ij} for Use in (12)

		j			
		0	1	2	3
i	0	-2.5053	-1.1081E-1	1.9189E-3	-1.3370E-5
	1	2.0822	4.7574E-3	-3.3316E-5	
	2	-5.9726E-1	-2.7550E-4		
	3	6.6112E-2			

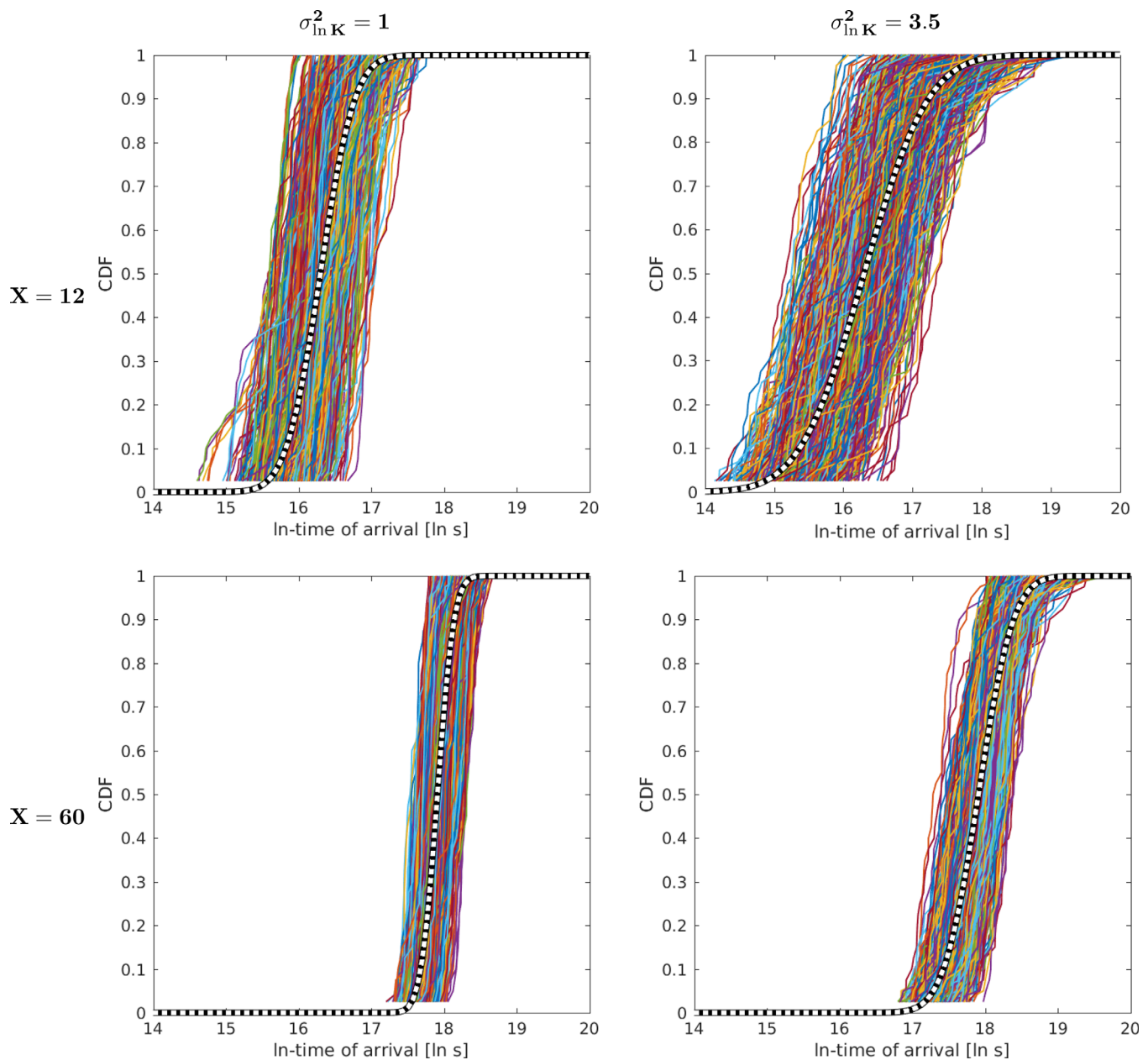


Figure 3. Each of the four plots shows the empirical breakthrough curves (expressed as arrival time CDFs) for approximately 1E3 randomly selected release points out of the 1E5 in single K -field realizations (thin, colored lines). Superimposed on each is the corresponding regression prediction using (12) (thick black-and-white-dashed lines). Plots in each column are from the same realization; plots in each row are from the same distance from the source. Note that the empirical breakthrough curves are truncated at the first particle arrival time and do not extend to zero.

for each value of $\sigma_{\ln K}^2$, at each distance downgradient of the source at which breakthrough curves are tabulated. In particular, it is noted that the largest divergence between breakthrough curves lies in their late-time tails. Consequently, the average (over the 10 realizations) variance of the natural logarithm of the 50% breakthrough time for each of the 100,000 release locations in that K -field realization is tabulated. This is shown in Figure 4. While an acceptable level of deviation will vary by application, it is apparent that as a function of $\sigma_{\ln K}^2$, the travel distance until a given deviation threshold is reached increases rapidly.

4.3. Convergence to Macrodispersion Theory

Above, we noted that at late times the predicted $\sigma_{\ln t}(X)$ of the breakthrough curves is less than 0.5 for all $\sigma_{\ln K}$ (see Figure 2). This means that the breakthrough at X is equally well modeled by an inverse Gaussian

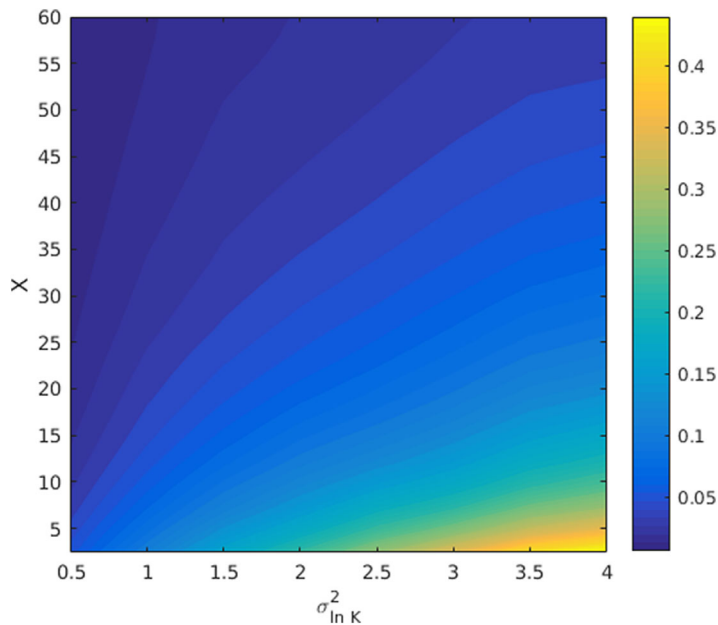


Figure 4. Color map of average (over all realizations) variance $\ln t$ for 50% breakthrough of the solute as function of distance from the source, X , and subsurface heterogeneity, $\sigma_{\ln K}^2$.

distribution (1), as it is by a lognormal distribution. Like the lognormal, the inverse Gaussian is determined by the first two moments of the arrival time, $t(X)$. Using (4), we may then predict the macrodispersion coefficient implied by the breakthrough curves at successive planes. The Fickian dispersion coefficient in an ADE model represents an intrinsic, local scattering propensity, and the concept of a plume-scale-dependent dispersion coefficient—though one of course may be fit to any plume—is not sensible in this context. Thus, it is reasonable to define the onset of the macrodispersion regime as the time at which D_∞ as determined by this equation no longer changes at planes with greater distances from the source. This was found to be a distance of $X = 40$, for all subsurface heterogeneity levels considered. (See Appendix B for further discussion.)

4.4. Comparisons With Existing Literature

To our knowledge, this is the first paper which calibrates a predictive relationship for breakthrough curve behavior before the macrodispersion regime, so we cannot directly compare with existing predictive models. However, to improve confidence in our results, we opted to demonstrate our flux-weighted breakthrough curve prediction against breakthrough curve data presented by another research group (Gotovac et al., 2009, Figure 4), for a single realization using a different numerical code. In Figure 5, we present the breakthrough data shown by Gotovac et al. to an upgradient pulse injection of solute into a randomly generated multi-Gaussian K -field with $\sigma_{\ln K}^2 = 1$, at three distances: $X = 10$, $X = 20$, and $X = 40$. Superimposed on these are the flux-weighted breakthrough curves determined via the regression calibrated from our study (12). The data in Gotovac et al. are expressed in terms of the dimensionless time, T , however the values of U and $l_{\ln K}$ were not specified in their paper, we were obligated to fit them. We found that the choice of $U = 1.05$, $l_{\ln K} = 1$ gave reasonable results, and these are the values used in Figure 5. Our prediction aligns relatively well with the Gotovac et al. data. As in our own study, we see that the prediction quality of our calibrated curves increase with X .

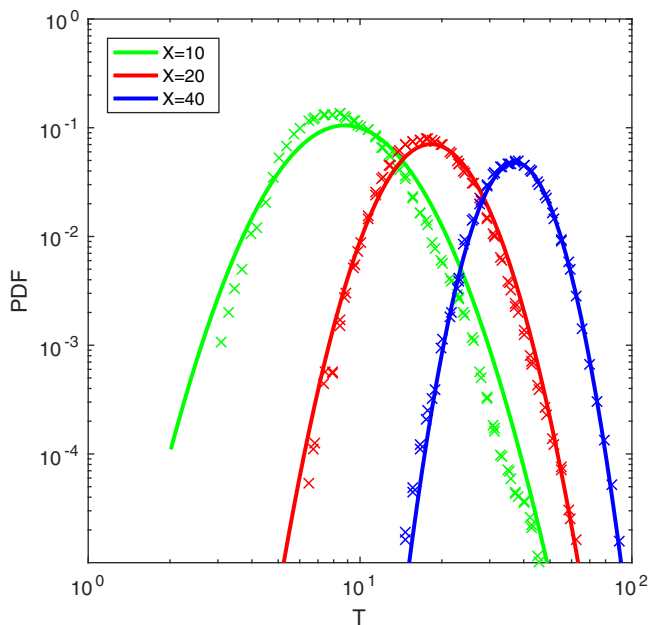


Figure 5. Simulated breakthrough data from a single realization with $\sigma_{\ln K}^2 = 1$ presented in Figure 4 of Gotovac et al. (2009; disconnected markers) compared with ensemble-averaged predictions using (12) (solid lines).

For the breakthrough curves in the macrodispersion regime, there is some prior art. In addition to the classic macrodispersion formula (5), Beaudoin and De Dreuzy (2013) performed a numerical study from which they propose a nondimensionalized empirical expression (their equation 9) for a late-time longitudinal macrodispersivity, α_∞ , which applies for $\sigma_{\ln K}^2$ greater than those for which the classical macrodispersion formula (5) is valid. Adapting it in terms of the quantities employed in this work is straightforward, as it follows from their definition of α_∞ that $D_\infty = \alpha_\infty l_{\ln K} U$. Using this relation allows us to rewrite their expression as

$$\frac{D_\infty}{l_{\ln K} U} = \exp\left(\frac{\sigma_{\ln K}^2}{1.55}\right). \tag{15}$$

A comparison of the late-time effective D_∞ determined from our computational study with two alternative expressions—the classical relation (5), and the more recent computationally derived equation (15)—is presented in Figure 6. Based on our results, usage of the classical relation appears valid at late time (equivalently, large distances from the source) for $\sigma_{\ln K}^2$ in the range $[0, 2]$. Beyond that point, our relation diverges, but increases more gently than the Beaudoin and de Dreuzy expression (15). Possible reasons for the discrepancy include our incorporation of local-scale dispersion and differing modeling assumptions.

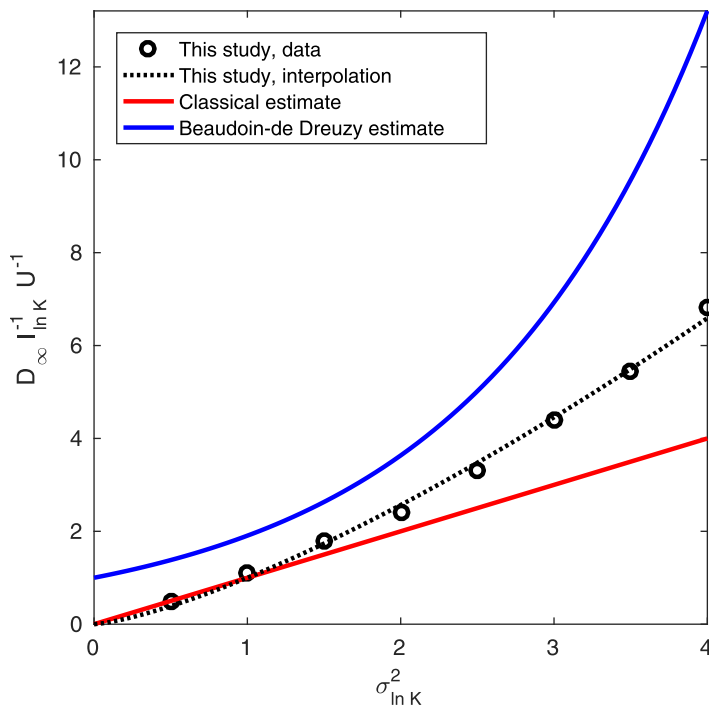


Figure 6. Comparison of the (nondimensionalized) late-time-implied macrodispersion coefficient, as computed from simulated breakthrough curve data in this study using equation (4) (black circles), as interpolated by (16) (black dotted curve), as estimated by the classical macrodispersion perturbation theory (5) (red curve), and as estimated by Beaudoin and de Dreuzy (15) (blue curve).

The macrodispersion coefficient derived from our simulations can be approximately interpolated by the following formula, as shown in Figure 6:

$$\frac{D_\infty}{I_{\ln K} U} = \sigma_{\ln K}^{2.72} \tag{16}$$

We note that on the right-hand side of this equation, we are conceptually taking the unit-independent quantity $\sigma_{\ln K}^2$ to the power 1.36, so both sides of the equation are effectively dimensionless.

5. Summary and Conclusions

The primary contribution of this paper has been the development of a predictive equation relating flux-weighted breakthrough curves in locally isotropic heterogeneous porous media to the underlying multi-Gaussian covariance structure of the log-hydraulic conductivity field, valid for larger conductivity field variability ($\sigma_{\ln K}^2 \leq 4$) and earlier (pre-asymptotic) times than the classical macrodispersion theory. The predictive equation, outlined in (12) and Table 1, has been obtained via polynomial regression on a large synthetic data set. Error estimates of the predicted flux-weighted breakthrough curves (which assume a large solute source extent transverse to mean flow) relative to point-release breakthrough curves have been presented. The theory presented here represents a way of predicting transition distributions in the RP-CTRW framework that would previously have required calibration against experimental data or have been without empirical grounding. It has also been observed that the macrodispersion theory, under highly dispersive conditions, provides grounding for the commonly supposed truncated power law form of the CTRW transition distribution (Appendix A).

A method for computing the macrodispersion coefficient from plane breakthrough data, rather than derivatives of whole-plume moments, has also been presented (4), and compared with an alternative approach (B2) in Appendix B, where estimates of the travel distance required for coefficients computed using these equations to reach their asymptotic values are also presented. Furthermore, (4) has been applied to the synthetic data set to determine an expression (16) for late-time macrodispersion that is valid for larger $\sigma_{\ln K}^2$ than the classic, perturbation-based macrodispersion theory. It was seen from this analysis that the classical theory obtains approximately for $\sigma_{\ln K}^2 < 2$. For larger values of $\sigma_{\ln K}^2$, a more mild increase in macrodispersion was found than in the recent work by Beaudoin and De Dreuzy (2013).

Given that previous studies have pointed in some different directions, we believe that further simulation studies using alternative numerical implementations and different assumptions would be beneficial for increasing confidence in underlying principles that have been identified. Non-Gaussian correlation structures have been found to have a significant impact on subsurface behavior (Haslauer et al., 2010, 2012) and exploring them in the context of solute breakthrough would throw light on the robustness of relationships developed using the Gaussian idealization. Furthermore, the interplay of local-scale dispersion and $\sigma_{\ln K}^2$ has a potentially important predictive role to play and has been little studied. These studies have been left for future work.

Appendix A: The Inverse Gaussian Distribution as Truncated Power Law

In (1), observe that the square-bracketed term is just the standard Gaussian spatial concentration profile, converted to a temporal density by the factor $\frac{x}{t}$. If the Gaussian is narrow, then x/t is approximately constant, and the breakthrough curve is quasi-Gaussian. To see the nature of the breakthrough curve when the Gaussian distribution defined in the brackets is wide, it is helpful to put the solution in a different form. We may rewrite (1) in terms of an alternative Peclet number, $\mathcal{P} \equiv \frac{Ux}{D}$, and dimensionless time, $\mathcal{T} \equiv \frac{Dt}{x^2}$. This yields

$$\frac{nU}{M} c_f(\mathcal{P}, \mathcal{T}) = \left[\frac{D}{x^2(4\pi)^{\frac{1}{2}}} \right] T^{-\frac{1}{2}} \exp\left\{ \frac{\mathcal{P}}{2} \right\} \exp\left\{ -\frac{\mathcal{P}^2 \mathcal{T}}{4} \right\} \exp\left\{ -\frac{1}{4\mathcal{T}} \right\}, \tag{A1}$$

where only the square-bracketed term is dimensional. In our problem, D , is constant, and for breakthrough at a fixed location, so is x . We note that for $\mathcal{T} \gg 1$,

$$c_f(\mathcal{P}, \mathcal{T}) \propto \mathcal{T}^{-\frac{1}{2}} \exp\left\{ -\frac{\mathcal{P}^2}{4} \mathcal{T} \right\}. \tag{A2}$$

This is to say, the breakthrough curve tail is a power law with exponential tempering. We see that if \mathcal{P} is small, the tempering term will be near unity, and one will be faced with significant power law behavior.

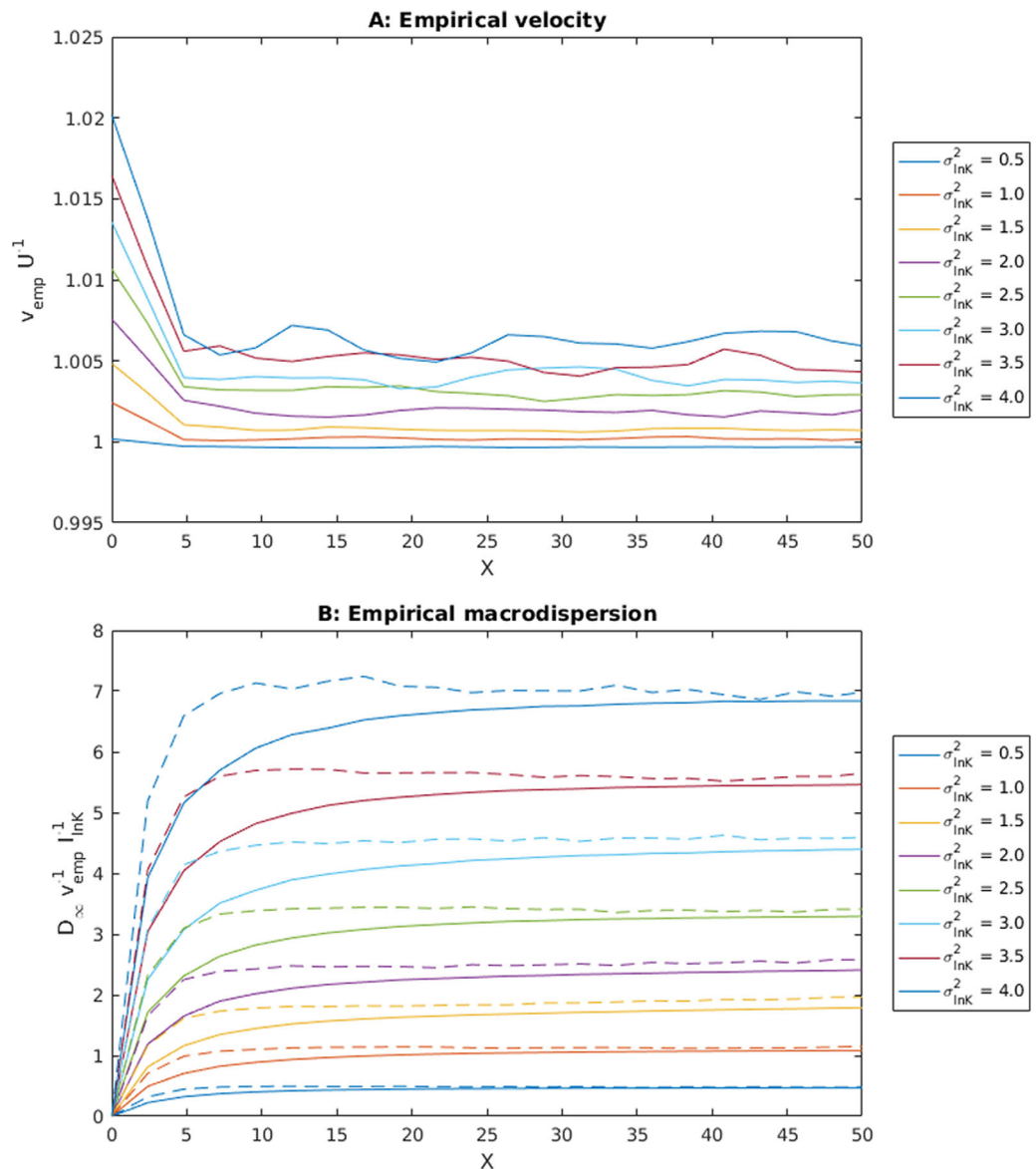


Figure B1. (a) Empirical flux-weighted solute velocity divided by mean groundwater flow velocity as a function of dimensionless distance from source. (b) Implied macrodispersion coefficient (4) (solid lines) and estimated ensemble macrodispersion a coefficient (B2) (dashed lines) as functions of dimensionless distance from source.

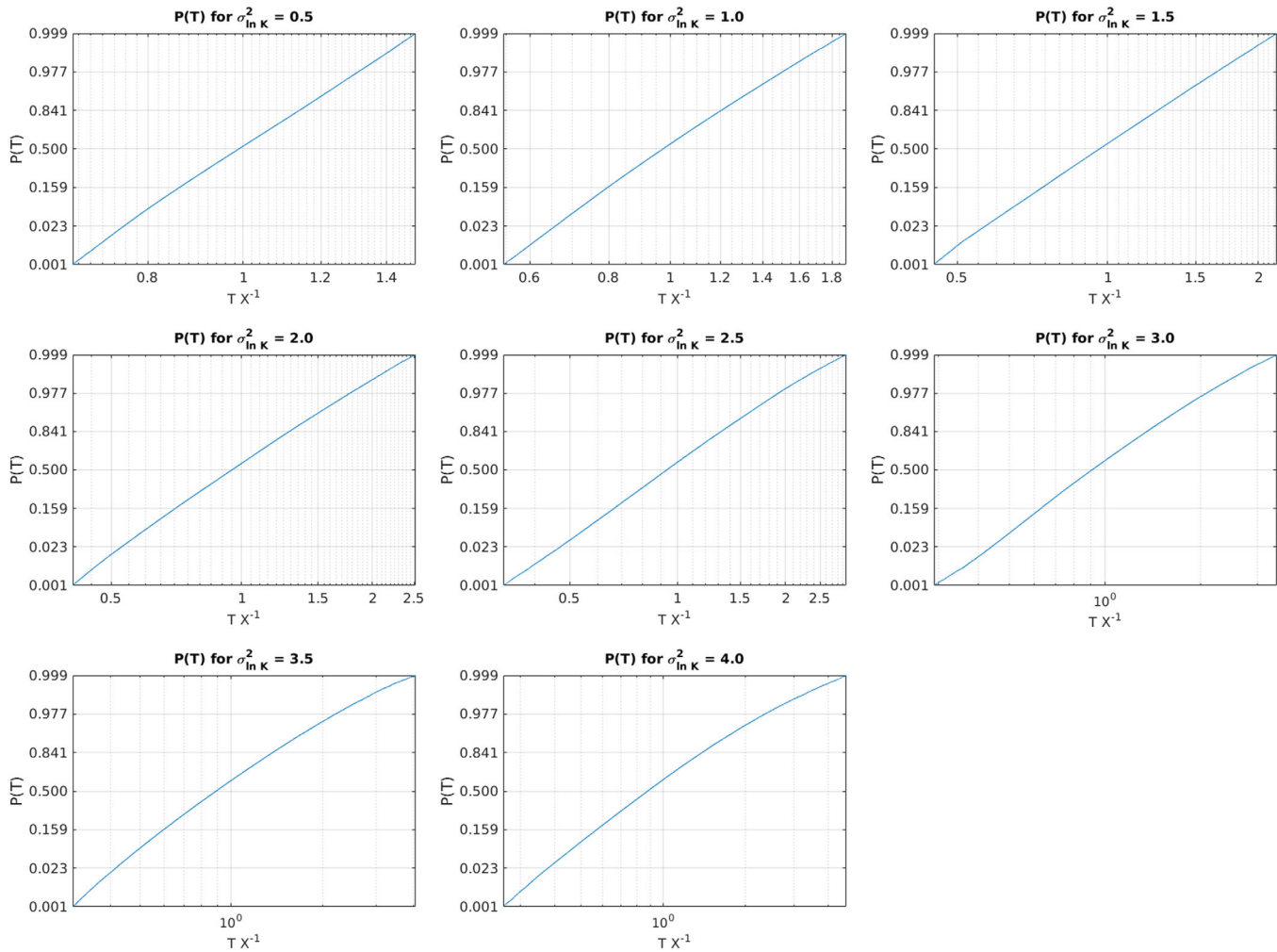


Figure C1. Probability plots of CDF, P , versus arrival time at $X = 48$ for eight values of $\sigma_{\ln K}^2$. Logarithmic scaling has been applied to each horizontal axis and inverse Normal scaling to each vertical axis, illustrating lognormality of arrival times.

Appendix B: Evolution of Empirical Velocity and Macrodispersion

We compute the first and second flux-weighted temporal moments for all planes at which breakthrough data was tabulated, respectively $m_1(x)$ and $m_2(x)$ and evaluate the second-central temporal moment $\sigma_t^2(x) = m_2(x) - m_1^2(x)$. Approximate spatial derivatives are computed at each plane by finite differences, which enables computation of empirical particle velocities and dispersion coefficients. Computation of empirical velocity, v_{emp} , is straightforward:

$$v_{\text{emp}} = \left(\frac{dm_1}{dx} \right)^{-1} \quad (\text{B1})$$

The variation of empirical velocity with distance is shown in Figure B1. It is apparent effective solute velocity closely matches U for all $\sigma_{\ln K}^2$, corroborating our approach and indicating that artificial dispersion into low- K regions is negligible in our simulations.

We next consider the definition of macrodispersion in terms of the solute plume second-central moment, $D_\infty \equiv \frac{1}{2} \frac{d\sigma_x^2}{dt}$. Assuming the plume to have a Gaussian profile in the direction of flow and a sufficiently small variance that we may use the approximation $\frac{x}{t} \approx U \approx v_{\text{emp}}$, we may, by inspection of (1), conclude that $\sigma_x^2 \approx v_{\text{emp}}^2 \sigma_t^2$. We can thus define the macrodispersion approximation

$$\tilde{D}_\infty = \frac{v_{\text{emp}}^3}{2} \frac{d\sigma_t^2}{dx}. \quad (\text{B2})$$

Both the implied D_∞ (4) and the approximation, \tilde{D}_∞ are shown as a function of distance in Figure B1. It is apparent that, regardless of how it is calculated, the macrodispersion coefficient stabilizes within the domain, indicating that our simulations are large enough to capture both preasymptotic and postasymptotic behavior. It is noteworthy, however, that the distance until the estimate of D_∞ stabilizes depends on how it is computed. The approximation based on plume moments approximates its asymptotic value by roughly $X = 10$, whereas the value implied by breakthrough curve behavior does so by $X = 40$. The implied macrodispersion expression is exact (4) and does not rely on spatial quadrature, whereas (B2), although approximate, is well defined in the preasymptotic regime. For large X (equivalently, large T), both the plume moment and breakthrough-curve-implied formulations are equivalent.

Appendix C: Verification of Breakthrough Curve Lognormality

Our regression (12) provides a prediction of the variance of log-arrival times, provided the dimensionless distance from the injection plane, X , and $\sigma_{\ln K}^2$. Coupled with the assumption of lognormality of breakthrough curves and an expression for mean arrival time, this is sufficient to completely specify the breakthrough curve. Here we evaluate the assumption of lognormality by selecting a fixed X , $X = 48$, and computing empirical flux-weighted CDFs of log-arrival time $\ln t$, $P(\ln t; \sigma_{\ln K}^2)$ for each $\sigma_{\ln K}^2$. If $N^{-1}(\cdot)$ is the inverse CDF for a normal distribution with the correct mean and variance, it follows that $N^{-1}(P(\ln t; \sigma_{\ln K}^2))$ will be a linear function of $\ln t$, and that a plot of P against t with suitable nonlinear axis scaling (respectively, according to N^{-1} and logarithmic) will be a straight line. We illustrate that this is (nearly) the case for all $\sigma_{\ln K}^2$ in Figure C1, indicating that the assumption of lognormal flux-weighted breakthrough curves is reasonable. As indicated in Gotovac et al. (2009), gradual loss of fidelity is seen in the tails with increasing $\sigma_{\ln K}^2$.

Acknowledgments

S.K.H. acknowledges the support of the Teach@Tübingen program and the LANL environmental programs. C.P.H. acknowledges the support of the DFG grant HA 7339/2-1. Numerical simulation data used to generate the figures have been archived by the corresponding author, and the MATLAB source code used to generate it has been included as supporting information.

References

- Banton, O., Delay, F., & Porel, G. (1997). A new time domain random walk method for solute transport in 1-D heterogeneous media. *Ground Water*, 35(6), 1008–1013.
- Beaudoin, A., & De Dreuzy, J. R. (2013). Numerical assessment of 3-D macrodispersion in heterogeneous porous media. *Water Resources Research*, 49, 2489–2496.
- Bellin, A., Rubin, Y., & Rinaldo, A. (1994). Eulerian-Lagrangian approach for modeling of flow and transport in heterogeneous geological formations. *Water Resources Research*, 30(11), 2913–2924.
- Bellin, A., Salandini, P., & Rinaldo, A. (1992). Simulation of dispersion in heterogeneous porous formations: Statistics, first-order theories, convergence of computations. *Water Resources Research*, 28(9), 2211–2227.
- Berkowitz, B., Cortis, A., Dentz, M., & Scher, H. (2006). Modeling non-Fickian transport in geological formations as a continuous time random walk. *Reviews of Geophysics*, 44, RG2003.
- Cvetkovic, V. (2011). The tempered one-sided stable density: A universal model for hydrological transport? *Environmental Research Letters*, 6(3), 034008.
- Cvetkovic, V., Cheng, H., & Wen, X.-H. (1996). Analysis of nonlinear effects on tracer migration in heterogeneous aquifers using Lagrangian travel time statistics. *Water Resources Research*, 32(6), 1671–1680.
- Cvetkovic, V., Fiori, A., & Dagan, G. (2014). Solute transport in aquifers of arbitrary variability: A time-domain random walk formulation. *Water Resources Research*, 50, 5759–5773.
- Cvetkovic, V., Shapiro, A. M., & Dagan, G. (1992). A solute flux approach to transport in heterogeneous formations: 2. Uncertainty analysis. *Water Resources Research*, 28(5), 1377–1388.
- Dagan, G. (1982). Stochastic modeling of groundwater flow by unconditional and conditional probabilities: 2. The solute transport. *Water Resources Research*, 18(4), 835–848.
- Dagan, G. (1989). *Flow and transport in porous formations*. Berlin, Germany: Springer.
- Dagan, G., Cvetkovic, V., & Shapiro, A. (1992). A solute flux approach to transport in heterogeneous formations: 1. The general framework. *Water Resources Research*, 28(5), 1369–1376.
- Dagan, G., & Fiori, A. (1997). The influence of pore-scale dispersion on concentration statistical moments in transport through heterogeneous aquifers. *Water Resources Research*, 33(7), 1595–1605.
- Dagan, G., Fiori, A., & Jankovic, I. (2003). Flow and transport in highly heterogeneous formations: 1. Conceptual framework and validity of first-order approximations. *Water Resources Research*, 39(9), 1268.
- Delay, F., & Bodin, J. (2001). Time domain random walk method to simulate transport by advection-dispersion and matrix diffusion in fracture networks. *Geophysical Research Letters*, 28(21), 4051–4054.
- Dentz, M., Cortis, A., Scher, H., & Berkowitz, B. (2004). Time behavior of solute transport in heterogeneous media: Transition from anomalous to normal transport. *Advances in Water Resources*, 27(2), 155–173.
- Dentz, M., Kinzelbach, H., Attinger, S., & Kinzelbach, W. (2000). Temporal behavior of a solute cloud in a heterogeneous porous medium: 1. Point-like injection. *Water Resources Research*, 36(12), 3591–3604.
- Dentz, M., Kinzelbach, H., Attinger, S., & Kinzelbach, W. (2002). Temporal behavior of a solute cloud in a heterogeneous porous medium: 3. Numerical simulations. *Water Resources Research*, 38(7).

- Di Dato, M., de Barros, F. P. J., Fiori, A., & Bellin, A. (2016). Effects of the hydraulic conductivity microstructure on macrodispersivity. *Water Resources Research*, *52*, 6818–6832.
- Dykaar, B. B., & Kitanidis, P. K. (1992). Determination of the effective hydraulic conductivity for heterogeneous porous-media using a numerical spectral approach: 1. Method. *Water Resources Research*, *28*(4), 1155–1166.
- Ederly, Y., Guadagnini, A., Scher, H., & Berkowitz, B. (2014). Origins of anomalous transport in heterogeneous media: Structural and dynamic controls. *Water Resources Research*, *50*, 1490–1505.
- Fiori, A. (1996). Finite Peclet extensions of Dagan's solutions to transport in anisotropic heterogeneous formations. *Water Resources Research*, *32*(1), 193–198.
- Fiori, A., & Jankovic, I. (2012). On preferential flow, channeling and connectivity in heterogeneous porous formations. *Mathematical Geosciences*, *44*(2), 133–145.
- Fiori, A., Zarlenga, A., Gotovac, H., Jankovic, I., Volpi, E., Cvetkovic, V., & Dagan, G. (2015). Advective transport in heterogeneous aquifers: Are proxy models predictive? *Water Resources Research*, *51*, 9577–9594.
- Gelhar, L. W., & Axness, C. L. (1983). Three-dimensional stochastic analysis of macrodispersion in aquifers. *Water Resources Research*, *19*(1), 161–180.
- Gotovac, H., Cvetkovic, V., & Andricevic, R. (2009). Flow and travel time statistics in highly heterogeneous porous media. *Water Resources Research*, *45*, W07402.
- Guadagnini, A. (2003). Mean travel time of conservative solutes in randomly heterogeneous unbounded domains under mean uniform flow. *Water Resources Research*, *39*(3), 1050.
- Haggerty, R., McKenna, S. A., & Meigs, L. C. (2000). On the late-time behavior of tracer test breakthrough curves. *Water Resources Research*, *36*(12), 3467–3479.
- Hansen, S. K., & Berkowitz, B. (2014). Interpretation and nonuniqueness of CTRW transition distributions: Insights from an alternative solute transport formulation. *Advances in Water Resources*, *74*, 54–63.
- Haslauer, C. P., Guthke, P., Bárdossy, A., & Sudicky, E. A. (2012). Effects of non-Gaussian copula-based hydraulic conductivity fields on macrodispersion. *Water Resources Research*, *48*, W07507.
- Haslauer, C. P., Li, J., & Bárdossy, A. (2010). Application of copulas in geostatistics. In *geoENV VII—Geostatistics for environmental applications* (pp. 395–404). Berlin, Germany: Springer.
- Janković, I., Fiori, A., & Dagan, G. (2003). Flow and transport in highly heterogeneous formations: 3. Numerical simulations and comparison with theoretical results. *Water Resources Research*, *39*(9), 1270.
- Kreft, A., & Zuber, A. (1978). On the physical meaning of the dispersion equation and its solutions for different initial and boundary conditions. *Chemical Engineering Science*, *33*(11), 1471–1480.
- Levy, M., & Berkowitz, B. (2003). Measurement and analysis of non-Fickian dispersion in heterogeneous porous media. *Journal of Contaminant Hydrology*, *64*(3–4), 203–226.
- Margolin, G., & Berkowitz, B. (2004). Continuous time random walks revisited: First passage time and spatial distributions. *Physica A: Statistical Mechanics and Its Applications*, *334*(1–2), 46–66.
- Moslehi, M., & de Barros, F. P. (2017). Uncertainty quantification of environmental performance metrics in heterogeneous aquifers with long-range correlations. *Journal of Contaminant Hydrology*, *196*, 21–29.
- Neuman, S. P., & Zhang, Y.-K. (1990). A quasi-linear theory of non-Fickian and Fickian subsurface dispersion theoretical analysis with application to isotropic media. *Water Resources Research*, *26*(5), 887–902.
- Pollock, D. W. (1988). Semianalytical computation of path lines for finite-difference models. *Ground Water*, *26*(6), 743–750.
- Rubin, S., Dror, I., & Berkowitz, B. (2012). Experimental and modeling analysis of coupled non-Fickian transport and sorption in natural soils. *Journal of Contaminant Hydrology*, *132*, 28–36.
- Rubin, Y. (2003). *Applied stochastic hydrogeology*. New York, NY: Oxford University Press.
- Rubin, Y., & Ezzedine, S. (1997). The travel times of solutes at the Cape Cod Tracer Experiment: Data analysis, modeling, and structural parameters inference. *Water Resources Research*, *33*(7), 1537–1547.
- Salandin, P., & Fiorotto, V. (1998). Solute transport in highly heterogeneous aquifers. *Water Resources Research*, *34*(5), 949–961.
- Schwartz, F. W. (1977). Macroscopic dispersion in porous media: The controlling factors. *Water Resources Research*, *13*(4), 743–752.
- Szrc, V., Cvetkovic, V., Andricevic, R., & Gotovac, H. (2013). Impact of aquifer heterogeneity structure and local-scale dispersion on solute concentration uncertainty. *Water Resources Research*, *49*, 3712–3728.
- Trefry, M. G., Ruan, F. P., & McLaughlin, D. (2003). Numerical simulations of preasymptotic transport in heterogeneous porous media: Departures from the Gaussian limit. *Water Resources Research*, *39*(3), 1063.
- Werth, C. J., Cirpka, O. A., & Grathwohl, P. (2006). Enhanced mixing and reaction through flow focusing in heterogeneous porous media. *Water Resources Research*, *42*, W12414.
- Woodbury, A. D., & Rubin, Y. (2000). A full-Bayesian approach to parameter inference from tracer travel time moments and investigation of scale effects at the Cape Cod Experimental Site. *Water Resources Research*, *36*(1), 159–171.
- Zech, A., Attinger, S., Cvetkovic, V., Dagan, G., Dietrich, P., Fiori, A., . . . Teutsch, G. (2015). Is unique scaling of aquifer macrodispersivity supported by field data? *Water Resources Research*, *51*, 7662–7679.